Journal of Power Sources 221 (2013) 122–127

Contents lists available at SciVerse ScienceDirect

Journal of Power Sources

journal homepage: www.elsevier.com/locate/jpowsour

Nitrogen-doped carbon coated $Li_4Ti_5O_{12}$ nanocomposite: Superior anode materials for rechargeable lithium ion batteries

Hongsen Li, Laifa Shen, Xiaogang Zhang*, Jie Wang, Ping Nie, Qian Che, Bing Ding

College of Material Science and Engineering, Nanjing University of Aeronautics and Astronautics, Yudao Street 29, Nanjing 210016, PR China

HIGHLIGHTS

- Carbon pre-coating process combined with ball milling.
- Smaller particles and narrower particle size distribution of NC–LTO.
- The NC–LTO exhibits obvious high rate capability and cycle stability.

ARTICLE INFO

Article history:
Received 4 April 2012
Received in revised form
20 June 2012
Accepted 13 August 2012
Available online 21 August 2012

Keywords:
Lithium ion battery
Nitrogen-doped carbon
Lithium titanate
High rate capability

ABSTRACT

Nitrogen-doped carbon coated $Li_4Ti_5O_{12}$ (NC–LTO) nanocomposite as an anode material for lithium-ion batteries (LIBs) is prepared with acetyl glucosamine as carbon source by pre-coating process combined with ball milling. X-ray diffraction, field emission scanning electron microscopy, transmission electron microscopy and X-ray photoelectron spectroscopy are used to characterize the NC–LTO materials. The results show that NC–LTO samples exhibit the obvious improvements in rate capability and cycling performance compared with the LTO samples coated by carbon (C–LTO) derived from sugar and pure LTO samples. The carbon pre-coating process could significantly decrease the agglomeration of TiO_2 precursors and the uniformly coated nitrogen-doped carbon increase the interfacial stability and electric conductivity of LTO. At the charge–discharge rate of 0.2 C, 5.0 C and 10.0 C and 20.0 C, the discharge capacities of NC–LTO samples are 167.4, 146.3, 133.4 and 128.2 mAh g^{-1}, respectively. After 1000 cycles at 1 C, its capacity retention is 95.9% with nearly ignored capacity fading.

1. Introduction

With growing concerns over limited oil resources and environmental issues, the need for clean and efficient energy storage has directed a global trend [1–5]. Lithium ion battery technology has attracted considerable attention owing to great potential to revolutionize the transportation industry [6–8]. However the current lithium-ion battery is handicapped by several critical disadvantages for large-scale applications for hybrid electric vehicles (HEVs) and electric vehicles (EVs), including low power density, short cycling life and safety hazards [2,7,8]. Therefore, the search for electrode materials with enhanced performance becomes one of the most important issues. Among the myriad electrode materials that have been studied, spinel $Li_4Ti_5O_{12}$ is an auspicious candidate in lithium ion batteries [9]. Compared with the general graphitic carbons anode materials, spinel $Li_4Ti_5O_{12}$ exhibits a flat and a relatively high lithium insertion/extraction voltage at about 1.55 V (vs. Li/Li^+) during charge and discharge, thus the formation of SEI layers and electroplating of lithium is avoiding [10]. Moreover, the spinel $Li_4Ti_5O_{12}$ shows excellent cycle life due to the negligible volume change, therefore it has been considered as a zero-strain material [11–16]. Besides, the spinel $Li_4Ti_5O_{12}$ has the high thermal stability, especially at elevated temperature. Unfortunately, $Li_4Ti_5O_{12}$ also suffers from poor electronic conductivity (10^{-13} S cm^{-1}) because of empty Ti 3d-states with a band gap energy of 2–3 eV results in an insulating character (electronic conductivity$<10^{-13}$ S cm^{-1}) to this material, which are the main problem that the electrochemical properties of $Li_4Ti_5O_{12}$ cannot commendably meet the requirements of the practical application [17].

To circumvent the above drawbacks of $Li_4Ti_5O_{12}$, several effective approaches have been proposed, such as nanosization [18–21], surface modification and doping with metal or non-metal ions in Li, Ti or O sites [22–24]. Decreasing the material particle size could reduce the Li^+ diffusion path and hence improve the rate capability of electrode materials. Surface modification by coating conductive species including Ag, carbon materials, SnO_2 and TiN, etc [25–27],

* Corresponding author. Tel.: +86 025 52112918; fax: +86 025 52112626.
E-mail address: azhangxg@163.com (X. Zhang).

0378-7753/$ – see front matter © 2012 Elsevier B.V. All rights reserved.
http://dx.doi.org/10.1016/j.jpowsour.2012.08.032

which improves the surface electronic conductivity and the electric contact between particles and conducting agents, thus improves electrochemical performance [28]. Our previous work has shown that with the doping of transition metal Nb, the electronic conductivity and electrochemical performance of $Li_4Ti_5O_{12}$ nanofibers was significantly improved [29]. Recently, a surface modification with nitrogen-doped carbon has attracted wide attention. It has been reported that nitrogen-doped carbon possesses many active defects which is beneficial for Li^+ diffusion. Hu and Dai's groups have recently used ionic liquids as precursors for the formation of nitrogen-doped carbon coatings on the electrode materials [30,31]. With a thin uniform coating layer formed on the surface of the materials, their electrochemical performances were improved prominently. While, with the consideration of the production cost and complexity, new precursors and methods still need to be research.

In this paper, we exploited a facile route to prepare nitrogen-doped carbon coated $Li_4Ti_5O_{12}$ nanocomposite by a carbon pre-coating process combined with ball milling which could make the samples more homogeneous over primary particles. The acetyl glucosamine was used as a carbon precursor, which contains elements of C, O, N, and H. The effects of carbon-free, carbon and N-doped carbon coatings on the electrochemical performance of $Li_4Ti_5O_{12}$ were investigated in detail. Such homogeneous distribution of the nitrogen-doped carbon and nano particle size afford a much better electrochemical performance, including an excellent rate capability and higher capacity.

2. Experimental

2.1. Synthesis

All of the reactants and solvents were of analytical grade and used without further purification. The NC–LTO was synthesized by using commercial crystalline anatase titania powders as raw materials and the N–doped carbon was derived from acetyl glucosamine. Typically, certain amounts of TiO_2, acetyl glucosamine and zirconia balls were mixed in alcohol and stirred by a planetary mill at a speed of 400 rpm for 2 h. The homogeneously mixed slurries were heat treated at 500 °C for 4 h under N_2 atmosphere for carbonization of acetyl glucosamine after drying with an infrared lamp. Then the resulted carbon-coated TiO_2 was ball milled in alcohol using the same speed with stoichiometric amounts of Li_2CO_3 for 4 h. Finally, the resulting slurry was dried and furthered calcined at 800 °C for 10 h under N_2 atmosphere. For comparison, the C-free and C–LTO (using sugar instead of acetyl glucosamine) samples were prepared using the same process.

2.2. Characterization

The microstructural properties of the resultant samples were obtained using emission scanning electron microscopy (SEM, HITACHI S-4800) and high-resolution transmission electron microscopy (TEM, JEOL JEM-2010). The crystal structure was characterized by X-ray diffraction (XRD) (Bruker D8 advance) with Cu Kα radiation. Thermogravimetric (TG) analyses were performed on a TG instrument (NETZSCH STA 409 PC) using a heating rate of 5 °C min^{-1} in an air atmosphere from 30 °C to 900 °C. The X-ray photoelectron spectroscopy (XPS) analysis was performed on a Perkin–Elmer PHI 550 spectrometer with Al Kα (1486.6 eV) as the X-ray source.

2.3. Electrochemical characterizations

Electrochemical evaluations were carried out by galvanostatic cycling in a CR2016-type coin cell. The working electrodes were formed by mixing 80 wt. % active materials, 10 wt. % carbon black, 10 wt. % polyvinylidene fluoride (PVDF) dissolved in N-methyl pyrrolidinone (NMP) and pasting the mixture on an aluminum foil current collector. Afterward, the electrode was dried under vacuum at 110 °C for 12 h. The cells were assembled with the cathode as prepared, lithium metal as anode and polypropylene (PP) film as separator. The electrolytes were 1 mol L^{-1} $LiPF_6$ solution in a 1:1 (V:V) mixture of ethylene carbonate (EC) and dimethyl carbonate (DMC). All the Test cells assembly process was in an argon-filled glove box. Galvanostatically charge–discharge experiments were performed at different current densities between 1.0 and 2.5 V (vs. Li/Li^+) using a CT2001A cell test instrument (LAND Electronic Co.).

3. Results and discussion

3.1. Structural characterizations

The high crystallinity and phase purity of the as-prepared pure LTO, C–LTO and NC–LTO are distinctly demonstrated by X-ray diffraction (XRD). As illustrated in Fig. 1, the identified peaks at 2θ = 18.4, 35.6, 43.3, 47.4, 57.2, 62.8, 66.1, 74.4 and 75.4°, corresponding to (111), (311), (400), (331), (333), (440), (531), (533) and (622) planes of a face-centered cubic spinel $Li_4Ti_5O_{12}$ with the Fd3m space group respectively which can be perfectly indexed to JCPDS card no. 49-0207. It is remarkable to note that in the case of C–LTO and NC–LTO, the addition of sugar and acetyl glucosamine has no effect on the crystal structure of spinel LTO. Besides, there is no obvious carbon detected in the XRD pattern, which is most likely due to the low content and/or the amorphous structure of carbon. While thermogravimetric (TG) analysis in Fig. 2 verify the presence of carbons in the C–LTO and NC–LTO samples, and the result demonstrate that the two samples almost have the same chemical composition of approximately 94.8% $Li_4Ti_5O_{12}$ and 5.2% carbon.

The morphology of the prepared pure LTO, C–LTO and NC–LTO samples is investigated by SEM. Fig. 3 shows the SEM images of the pure LTO, C–LTO and NC–LTO samples obtained at 800 °C for 10 h. As seen in the images, the morphology of the pure LTO samples (Fig. 3a) is disordered and the particles size distribution is rather wide ranging from 50 to 400 nm. However, the typical size of the prepared C–LTO and NC–LTO is uniform and in a narrow range 50–200 nm (which is measured using the dynamic and static light-scattering detector) as seen in Fig. 3b and c respectively.

To further examine the architecture of the pure LTO, C–LTO and NC–LTO, the samples are investigated by TEM as seen in Fig. 4. It can be clearly seen that the NC–LTO (Fig. 4a, b) and C–LTO (Fig. 4c) samples are coated by a thin carbon layer, and the surface of the

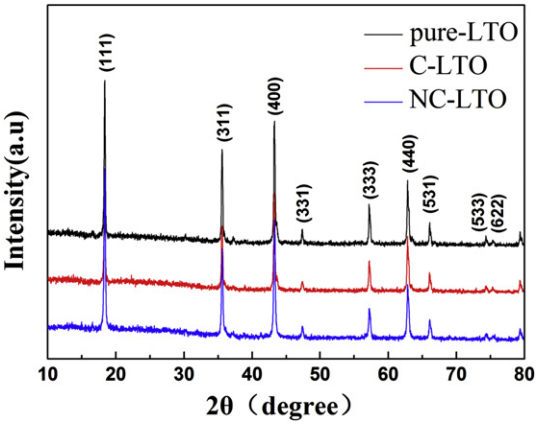

Fig. 1. Typical XRD patterns of pure LTO, C–LTO and NC–LTO.

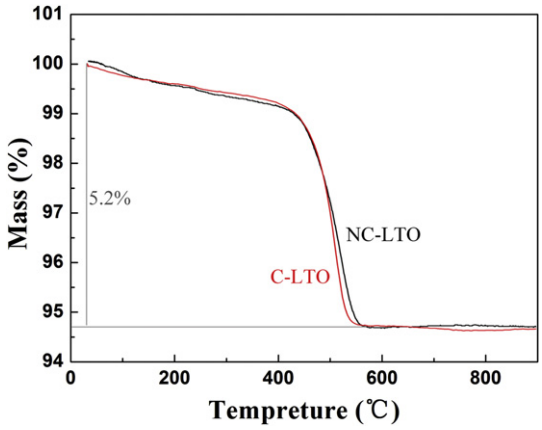

Fig. 2. TG curves of the NC–LTO and C–LTO measured from 30 to 900 °C in air flow with a heating rate of 5 °C min^{-1}.

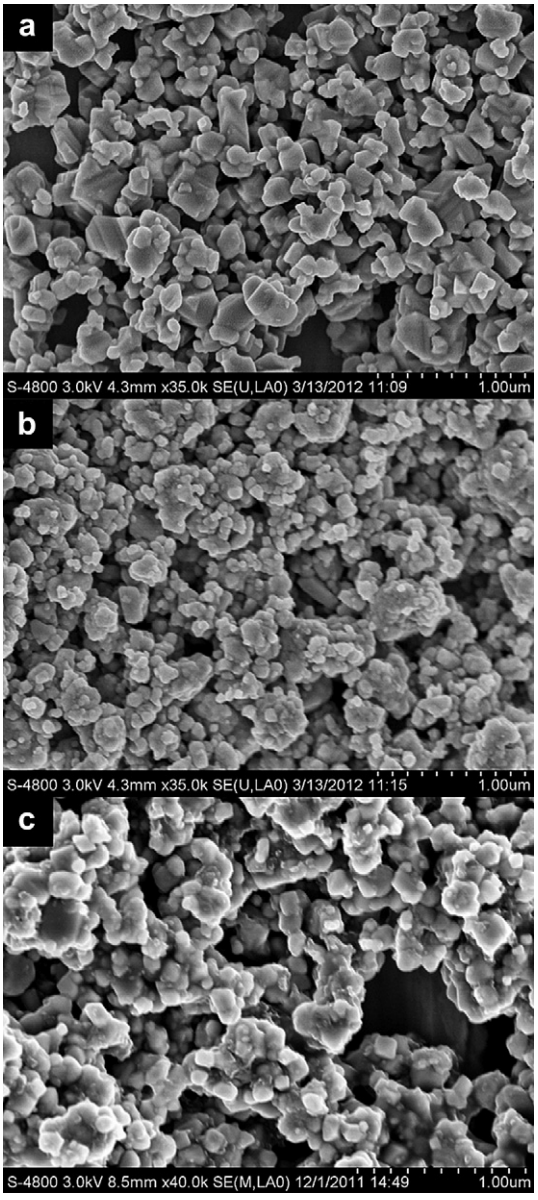

Fig. 3. SEM images of pure LTO (a) C–LTO (b) and NC–LTO (C).

pure LTO (Fig. 4d) is quite smooth. The presence of the surface carbon layer for NC–LTO and C–LTO resulting from carbonization of acetyl glucosamine and sugar respectively, it can restrain the growth of the $Li_4Ti_5O_{12}$ crystalline grains during solid-state sintering and thereby control their size on the nano-meter scale, as observed in the SEM images of Fig. 3b and c. Meanwhile, the uniform distribution of carbon could also decreases the degree of agglomeration of the particles and establishes a conductive network through the whole material which is favorable for lithium ion transport across the interface between the active materials and electrolyte [25]. The HRTEM image (see Fig. 4b) clarifies the crystal structure, with an interplanar spacing revealed of approximately 0.48 nm between neighboring [111] planes of spinel-type NC–LTO.

The XPS survey spectra of NC–LTO, C–LTO and pure LTO samples are shown in Fig. 5a. It can be clearly to see that a new peak at around 399 eV which can be ascribed to N 1s was appeared in the NC–LTO survey spectra, while it cannot be detected for the C–LTO and pure LTO samples, suggesting the presence of N in NC–LTO samples. Moreover, the intensity of the C 1s peak in the obtained pure LTO samples are much lower than the NC–LTO and C–LTO samples, which is owing to the carbon coating on their outer surface. The elemental C in pure LTO may be ascribed to residual carbon from its precursor and adventitious hydrocarbons from the XPS instrument itself and it was also reported elsewhere [32]. Fig. 5b shows the typical high-resolution XPS spectra of N 1s for the NC–LTO. The two peaks at around 398 and 401 eV was corresponded to C–N and C═N respectively [33]. According to the ref [28], the appearance of the C–N and C═N could lead to defects in the graphite structure and the existence of defects introduced by N-doping would be beneficial for Li^+ diffusion in the interface. Besides, the peak at around 397 eV was belonged to Ti–N [34], perhaps caused by the Ti–N–C-like species [31].

The elemental analysis (CHN–O-Rapid) was used to detect the detail compositions of the prepared pure LTO, C–LTO and NC–LTO samples. The result was summarized in Table 1. From the data of the table, it can be seen that the mass ratio of the element C of the C–LTO and NC–LTO samples was appropriate 5.2%, which was consistent with the TG result. The mass ratio of the element N of the NC–LTO sample was 0.34% which demonstrate that the element N of the precursor acetyl glucosamine can be remained a satisfy value after treated at 800 °C for 10 h.

3.2. Electrochemical measurements

Fig. 6 displays the typical discharge/charge profiles of the NC–LTO samples cycled under different current density between the voltage limits of 1.0–2.5 V. The discharge current rates vary from 0.2 C to 20.0 C. At the initial lower rate of 0.2 C, the NC–LTO samples give a discharge capacity of 167.4 mAh g^{-1}, which is close to its theoretical capacity of 175 mAh g^{-1}. Moreover, the sample shows a very flat charge/discharge plateau at the potential of around 1.55 V (*vs.* Li/Li^+), which corresponded to the reversible phase transition between $Li_4Ti_5O_{12}$ and $Li_7Ti_5O_{12}$ [35]. As the discharge–charge rate increases from 1.0 C to 20.0 C, the discharge capacities of NC–LTO samples were slightly reduced and it delivered 160.3, 157.1, 146.3, 137.4, 133.4, 128.2 mAh g^{-1} at the rate of 1.0 C, 2.0 C, 5.0 C, 8.0 C, 10.0 C and 20.0 C, respectively. It is noteworthy that even at the high rate of 20.0 C, the NC–LTO samples still shows capacity retention as high as 76.6%, demonstrating a remarkable rate capability.

Fig. 7 shows the discharge/charge profiles of the NC–LTO, C–LTO and pure LTO samples at the rate of 1.0 C and the discharge capacities of the three samples are 160.5, 153.5 and 149.6 mAh g^{-1} respectively. The polarization between the discharge and charge plateau for the NC–LTO samples is 63 mV which is much lower

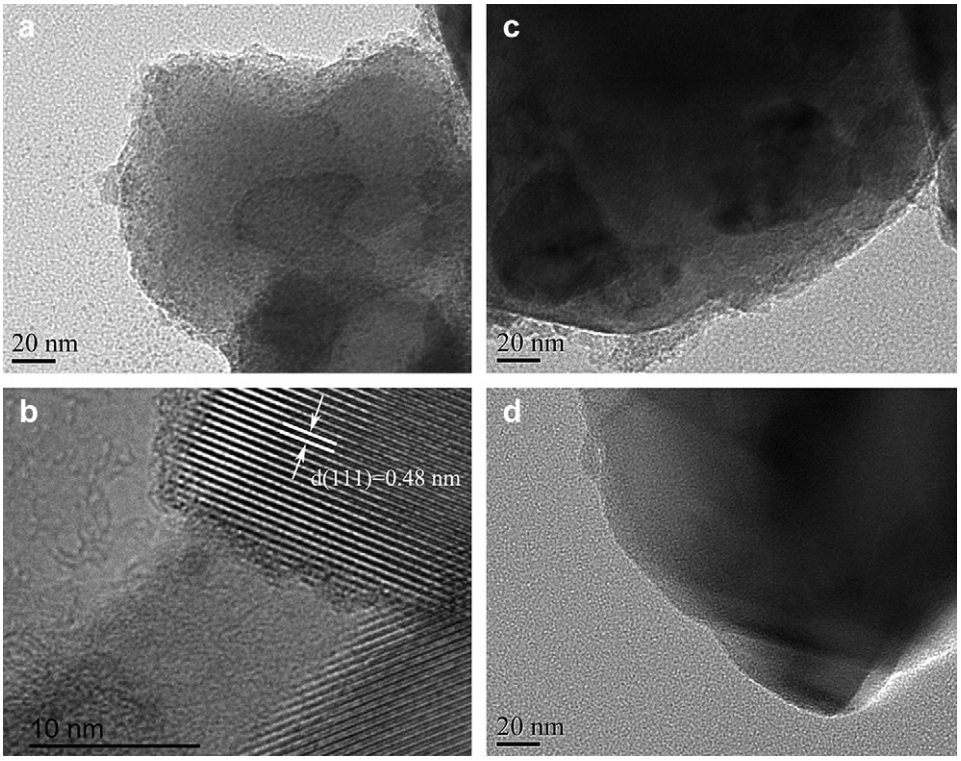

Fig. 4. TEM images of NC–LTO (a), C–LTO (c), pure LTO (d) and HRTEM images of NC–LTO (b) after calcinations in N_2 at 800 °C for 10 h.

compared to the C–LTO samples (78 mV) and the pure LTO samples (146 mV). The lower polarization for the NC–LTO samples was attributed to the better reaction kinetics, which indicates that the improved electrical conductivity after N-doped carbon coatings.

Fig. 8 compares the rate capability of the pure samples, carbon-coated samples and the N-doped carbon coated samples with different carbon contents. At a low rate of 0.2 C, all samples deliver nearly the same discharge capacities, but the pure LTO shows a little higher capacities. However, at higher rates of 5.0 C and 10.0 C, the discharge capacities of pure LTO dropped dramatically, 56.2, 12.5 mAh g^{-1}, respectively. At the same rates, the corresponding values for C–LTO and 5.2% NC–LTO (5.2% carbon contents) were 132.1, 115.0 and 146.3, 133.2 mAh g^{-1}, respectively. Interestingly, the capacities of the 5.2% NC–LTO (133.2 mAh g^{-1}) at rate of 10.0 C were a little lower than the capacities of the pure LTO (149.4 mAh g^{-1}) at rate of 1.0 C and higher than the capacities of the C–LTO (132.1 mAh g^{-1}) at rate of 5.0 C. The carbon contents effect on the reversible capacities of NC–LTO was also studied. As shown in Fig. 8, when the carbon contents increased from 5.2% to 7.6%, the reversible capacities did not show an improvement. The thickness of the coating layer increased with the carbon contents, which may restrict the efficient charge transfer/transport. In addition, we also performed further experiments to decrease the carbon contents in the composite, no surprisingly, the capacities were reduced because it could not form a uniform coating layer, thus a continuous electronic conducting network being formed in the composite is critical to improve the electrochemical performance which was also reported elsewhere [31].

Despite the superior rate capability, the NC–LTO samples also reveal excellent cycling performance. The cycling performance of the pure samples, carbon and the N-doped carbon coating samples at 1.0 C in a half cell is shown in Fig. 9. In the case of NC–LTO

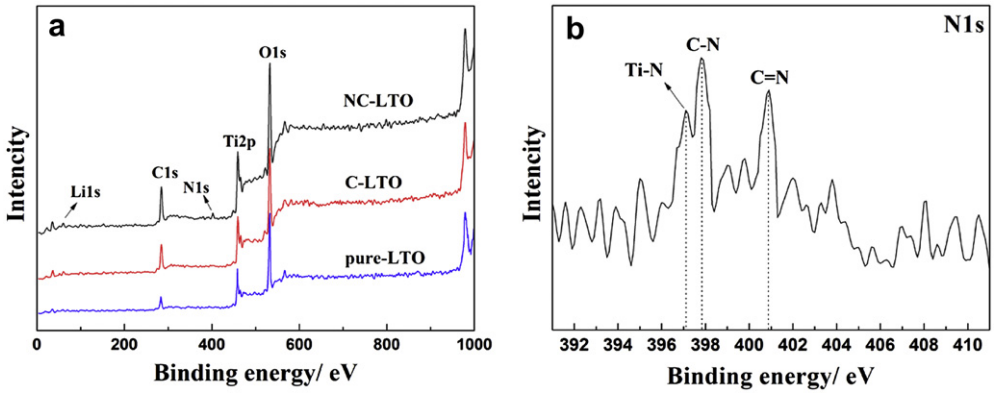

Fig. 5. XPS survey spectrums of NC–LTO, C–LTO, pure LTO (a) and typical high-resolution XPS spectra of N 1s for the NC–LTO (b).

Table 1
Mass ratio of the element C, H, N in the samples.

Samples	C% (mass%)	H% (mass%)	N% (mass%)
NC–LTO	5.13	0.11	0.34
C–LTO	5.16	0.06	0.00
Pure LTO	0.00	0.00	0.00

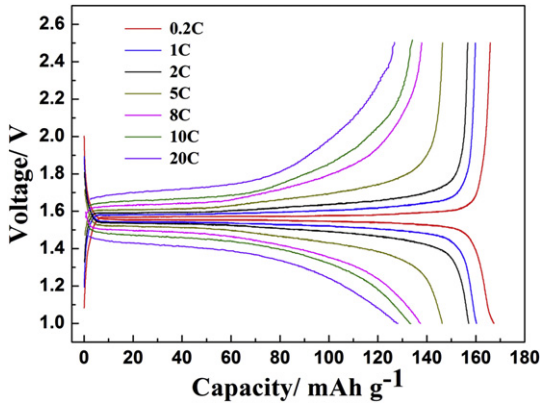

Fig. 6. Galvanostatic charge–discharge curves for the NC–LTO between 1.0 and 2.5 V at different current densities.

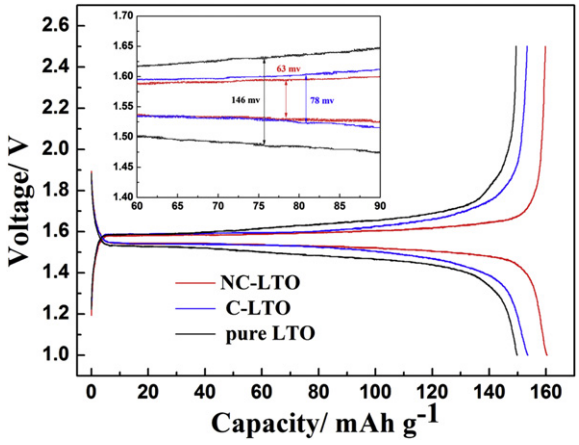

Fig. 7. The discharge/charge curves of NC–LTO, C–LTO and pure LTO samples at the rate of 1.0 C.

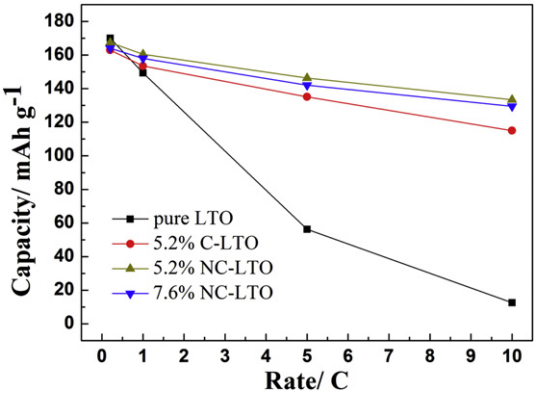

Fig. 8. The rate capabilities of C–LTO and NC–LTO samples compared with the pure LTO sample.

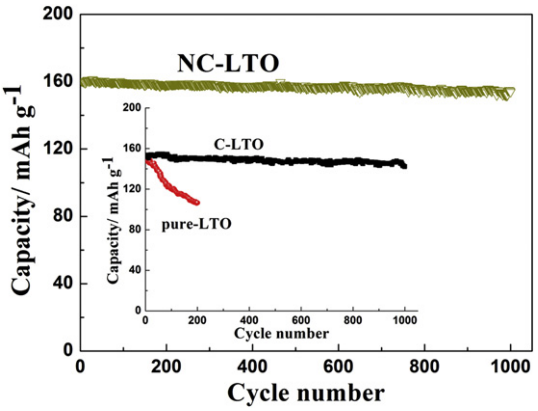

Fig. 9. Cycling performance of NC–LTO. Inset: The cycling performance of C–LTO and pure LTO.

samples, after 1000 cycles, it demonstrates remarkable cycling stability by delivering the discharge capacity of 153.9 mAh g^{-1} with capacity retention of 95.9%. For the C–LTO samples, the initial capacity was 153.6 mAh g^{-1}, which decreased to 141.8 mAh g^{-1} after 1000 cycles with capacity retention of 92.3%. However the pure samples gave an initial capacity of 149.5 mAh g^{-1} and the values reduced to 106.6 mAh g^{-1} after 200 cycles with capacity retention of 71.3%. This further confirms the advantage of the use of N-doped carbon as a coating layer for LTO electrodes.

4. Conclusions

In summary, we have demonstrated an efficient approach to prepare nitrogen-doped carbon coating nanosized $Li_4Ti_5O_{12}$ (NC–LTO). When evaluated as an anode material for LIBs, the NC–LTO samples with a uniform layer exhibit enhancement of high rate capability and high stability for lithium storage compared with the C–LTO and pure LTO. At rate of 20.0 C, NC–LTO samples shows the discharge capacities of 128.2 mAh g^{-1} with capacity retention as high as 76.6%. Besides, after 1000 cycles at 1.0 C, the capacity retention of NC–LTO samples was 95.9% with nearly ignored capacity fading. The superior electrochemical performance of NC–LTO was attributed to the nanosized $Li_4Ti_5O_{12}$ particles and nitrogen-doped carbon uniformly coatings that enable the fast ion and electron transport. We anticipate that such nitrogen-doped carbon surface modified LTO could be a promising anode material for high-rate lithium ion batteries.

Acknowledgments

This work is financially supported in part by the National Natural Science Foundation of China (21173120), Natural Science Foundation of Jiangsu Province (BK2011030) and Specialized Research Fund for the Doctoral Program of Higher Education of China (No. 20060287026). L.S. would also like to thank the Jiangsu Innovation Program for Graduate Education (CXZZ11_0204) and Outstanding Doctoral Dissertation in NUAA (BCXJ11-10).

References

[1] H.G. Jung, S.T. Myung, C.S. Yoon, S.B. Son, K.H. Oh, K. Amine, B. Scrosati, Y.K. Sun, Energy Environ. Sci. 4 (2011) 1345–1351.
[2] S.L. Chou, J.Z. Wang, H.K. Liu, S.X. Dou, J. Phys. Chem. C 115 (2011) 16220–16227.
[3] L.F. Shen, X.G. Zhang, H.S. Li, C.Z. Yuan, G.Z. Cao, J. Phys. Chem. Lett. 2 (2011) 3096–3101.
[4] D. Lepage, C. Michot, G.X. Liang, M. Gauthier, S.B. Schougaard, Angew. Chem. 123 (2011) 7016–7019.
[5] S.W. Kim, D.H. Seo, H. Gwon, J. Kim, K. Kang, Adv. Mater. 22 (2010) 5260–5264.

[6] L. Cheng, J. Yan, G.N. Zhu, J.Y. Luo, C.X. Wang, Y.Y. Xia, J. Mater. Chem. 20 (2010) 595–602.
[7] Z.D. Huang, X.M. Liu, S.W. Oh, B. Zhang, P.C. Ma, J.K. Kim, J. Mater. Chem. 21 (2011) 10777–10784.
[8] L.F. Shen, C.Z. Yuan, H.J. Luo, X.G. Zhang, K. Xu, Y.Y. Xia, J. Mater. Chem. 20 (2010) 6998–7004.
[9] M. Masatoshi, U. Satoshi, Y. Eriko, K. Keiji, I. Shinji, J. Power Sources 101 (2001) 53–59.
[10] T. Ohzuku, A. Ueda, N. Yamamoto, J. Electrochem. Soc. 142 (1995) 1431–1435.
[11] K. Ariyoshi, R. Yamato, T. Ohzuku, Electrochim. Acta 51 (2005) 1125.
[12] M.M. Thackeray, J. Electrochem Soc. 142 (1995) 2558–2563.
[13] L. Aldon, P. Kubiak, M. Womes, J.C. Jumas, J. Olivier-Fourcade, J.L. Tirado, J.I. Corredor, C.P. Vicente, Chem. Mater. 16 (2004) 5721–5725.
[14] K.M. Colbow, J.R. Dahn, R.R. Haering, J. Power Sources 26 (1989) 397–402.
[15] A. Guerfi, S. Sevigny, M. Lagace, P. Hovington, K. Kinoshita, K. Zaghib, J. Power Sources 88 (2003) 119–121.
[16] L.F. Shen, C.Z. Yuan, H.J. Luo, X.G. Zhang, L. Chen, H.S. Li, J. Mater. Chem. 21 (2011) 14414–14416.
[17] P.P. Prosini, R. Mancini, L. Petrucci, V. Contini, P. Villano, Solid State Ionics 144 (2001) 185–192.
[18] A. Guerfi, P. Charest, K. Kinoshita, M. Perrier, K. Zaghib, J. Power Sources 126 (2004) 163–168.
[19] J. Lim, E. Choi, V. Mathew, D. Kim, D. Ahn, J. Gim, S.H. Kang, J. Kima, J. Electrochem. Soc. 158 (2011) A275–A280.
[20] A.S. Prakash, P. Manikandan, K. Ramesha, M. Sathiya, J.M. Tarascon, A.K. Shukla, Chem. Mater. 22 (2010) 2857–2863.
[21] J. Lu, C.Y. Nan, Q. Peng, Y.D. Li, J. Power Sources 202 (2012) 246–252.
[22] T.F. Yi, J. Shu, Y.R. Zhu, X.D. Zhu, R.S. Zhu, A.N. Zhou, J. Power Sources 195 (2010) 285–288.
[23] A.D. Robertson, L. Trevino, H. Tukamoto, J.T.S. Irvine, J. Power Sources 81–82 (1999) 352–357.
[24] H.M. Xie, R.S. Wang, J.R. Ying, L.Y. Zhang, A.F. Jalbout, H.Y. Yu, G.L. Yang, X.M. Pan, Z.M. Su, Adv. Mater. 18 (2006) 2609–2613.
[25] G.N. Zhu, H.J. Liu, J.H. Zhuang, C.X. Wang, Y.G. Wang, Y.Y. Xia, Energy Environ. Sci. 4 (2011) 4016–4022.
[26] G.J. Wang, J. Gao, L.J. Fu, N.H. Zhao, Y.P. Wu, T. Takamura, J. Power Sources 174 (2007) 2009–2112.
[27] L.J. Fu, H. Liu, H.P. Zhang, C. Li, T. Zhang, Y.P. Wu, R. Holze, H.Q. Wu, Electrochem. Commun. 8 (2006) 1–4.
[28] Z.J. Ding, L. Zhao, L.M. Suo, Y. Jiao, S. Meng, Y.-S. Hu, Z.X. Wang, L.Q. Chen, Phys. Chem. Chem. Phys. 13 (2011) 15127–15133.
[29] H.S. Li, L.F. Shen, X.G. Zhang, P. Nie, L. Chen, K. Xu, J. Electrochem. Soc. 159 (2012) A426–A430.
[30] S. Yoon, C. Liao, X.G. Sun, C.A. Bridges, R.R. Unocic, J. Nanda, S. Dai, M.P. Paranthaman, J. Mater. Chem. 22 (2012) 4611–4614.
[31] L. Zhao, Y.S. Hu, H. Li, Z.X. Wang, L.Q. Chen, Adv. Mater. 23 (2011) 1385–1388.
[32] Y.G. Wang, H.M. Liu, K.X. Wang, H. Eiji, Y.R. Wang, H.S. Zhou, J. Mater. Chem. 19 (2009) 6789–6795.
[33] S. Bhattacharyya, C. Cardinaud, G. Turban, J. Appl. Phys. 83 (1998) 4491–4500.
[34] N.C. Saha, H.G. Tompkins, J. Appl. Phys. 72 (1992) 3072–3079.
[35] H.S. Zhou, D.L. Li, M. Hibino, I. Honma, Angew. Chem. Int. Ed. 44 (2005) 797–802.